

The Modeling and Harmonic Coupling Analysis of Multiple-Parallel Connected Inverter Using Harmonic State Space (HSS)

Kwon, Jun Bum; Wang, Xiongfei; Bak, Claus Leth; Blaabjerg, Frede

Published in:

Proceedings of the 2015 IEEE Energy Conversion Congress and Exposition (ECCE)

DOI (link to publication from Publisher):

[10.1109/ECCE.2015.7310534](https://doi.org/10.1109/ECCE.2015.7310534)

Publication date:

2015

Document Version

Accepted author manuscript, peer reviewed version

[Link to publication from Aalborg University](#)

Citation for published version (APA):

Kwon, J. B., Wang, X., Bak, C. L., & Blaabjerg, F. (2015). The Modeling and Harmonic Coupling Analysis of Multiple-Parallel Connected Inverter Using Harmonic State Space (HSS). In *Proceedings of the 2015 IEEE Energy Conversion Congress and Exposition (ECCE)* (pp. 6231-6238). IEEE Press.
<https://doi.org/10.1109/ECCE.2015.7310534>

General rights

Copyright and moral rights for the publications made accessible in the public portal are retained by the authors and/or other copyright owners and it is a condition of accessing publications that users recognise and abide by the legal requirements associated with these rights.

- Users may download and print one copy of any publication from the public portal for the purpose of private study or research.
- You may not further distribute the material or use it for any profit-making activity or commercial gain
- You may freely distribute the URL identifying the publication in the public portal -

Take down policy

If you believe that this document breaches copyright please contact us at vbn@aub.aau.dk providing details, and we will remove access to the work immediately and investigate your claim.

The Modeling and Harmonic Coupling Analysis of Multiple-Parallel Connected Inverter Using Harmonic State Space (HSS)

JunBum Kwon, Xiongfei Wang, Claus Leth Bak, Frede Blaabjerg
Department of Energy Technology
Aalborg University
Aalborg, Denmark
E-mail : jbk, xwa, clb, fbl @et.aau.dk

Abstract—As the number of power electronics based systems are increasing, studies about overall stability and harmonic problems are rising. In order to analyze harmonics and stability, most research is using an analysis method, which is based on the Linear Time Invariant (LTI) approach. However, this can be difficult in terms of complex multi-parallel connected systems, especially in the case of renewable energy, where possibilities for intermittent operation due to the weather conditions exist. Hence, it can bring many different operating points to the power converter, and the impedance characteristics can change compared to the conventional operation. In this paper, a Harmonic State Space modeling method, which is based on the Linear Time varying theory, is used to analyze different operating points of the parallel connected converters. The analyzed results show that the HSS modeling approach explicitly can demonstrate other phenomenon, which can not be found in the conventional LTI approach. The theoretical modeling and analysis are verified by means of simulations and experiments.

Keywords—Harmonic State Space Modeling, Multi-parallel connected inverter, Harmonic instability, power converters, renewable energies

I. INTRODUCTION

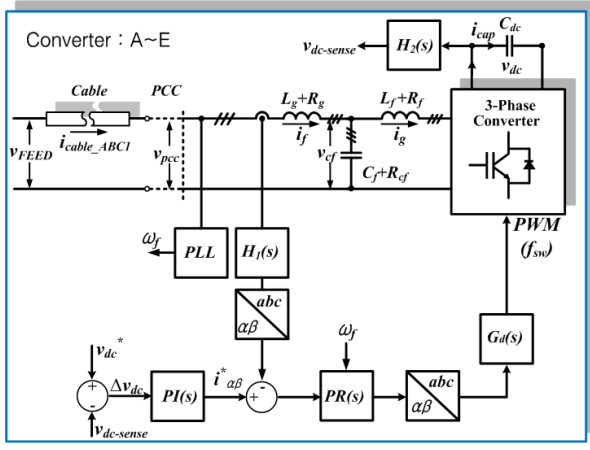
The paradigm for harmonic and stability analysis of power converter is now changing from a single power converter to multi-connected power converters, as the number of renewable energy and power electronics based systems [2] are increasing. Hence, it is required to find proper modeling and analysis methods because of the complexity of the power converter and system network. Conventionally, Linear Time Invariant (LTI) based models are used with the assumption that the switching frequency is high and the operating point is not changing. As a result, the analysis of the grid connected converters is performed based on the LTI-based state-space model [3, 4]. Besides various kind of models are used in order to detect faults in the system [5, 6]. [7] The generalized averaging [8], and the harmonic linearization methods [9] are proposed to map the limitations of the LTI model.

However, the stability and harmonic analysis are mainly done by studying at a single frequency and there are no methods to explain the dynamic and steady-state coupling between the AC dynamics and the DC dynamics of the power electronics systems. Practically the operating point of the

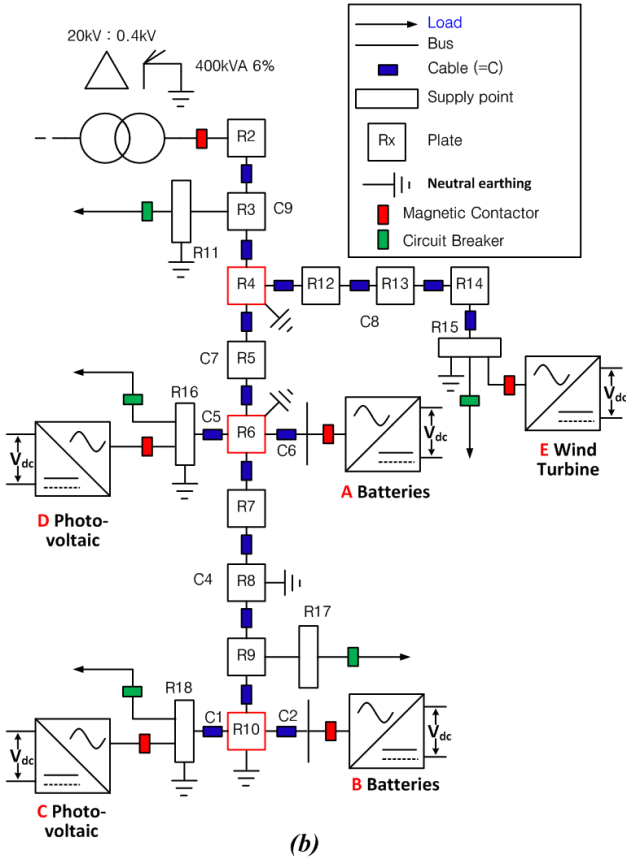
power converter is also changing continuously. One example is that the wind power converters in a wind farm which have experienced such phenomenon due to the wake effect of the wind, different operating point of each converter and disconnection happened by the protection [10]. This practical operation is still uncertain in power converter analysis [11] because of these characteristics. Furthermore, such phenomenon can make the harmonic and resonance analysis difficult. Hence, it is required to develop the advanced models, which can consider these varying operating points for a detailed study.

To overcome this challenge and to show other harmonic impedance couplings in the system, the Harmonic State Space (HSS) modeling method [12] is introduced for power system studies. Based on the theory of Harmonic Domain (HD) [13], Extended Harmonic Domain (EHD) [14], and Harmonic Transfer Function (HTF) [15], the HSS modeling method is developed in order to analyze the harmonic coupling and stability with individual harmonic impedances. Before used in power system analysis, it has been able to determine mechanical resonances of wind turbine blades, blade analysis of helicopters and also structure resonance analysis of bridges to figure out the uncertain characteristics, which can not be found by the conventional LTI modeling approach [16, 17].

This paper proposes a model for multi-parallel connected power converters using the HSS modeling method. First, the modelling procedure for single converters is explained briefly including a review of the HSS modeling. The important characteristics are that the harmonic impedance of the converter is varying according to the operating point. This characteristic is quite noticeable in the application of high-power converter using low switching frequency. Second, the multi-parallel connected inverter modeling is implemented based on the results of single 3-phase converter and cable modeling. Furthermore, in order to enhance the validity of the modeling, a Cigre-Bench mark model for low voltage micro-grid is used as a reference [1]. Next, the steady-state impedance coupling and dynamic impedance coupling characteristic between the converters are analyzed by means of the HD and the HTF modeling. The analyzed results are verified by time-domain and the frequency domain simulations as well as experimental results.



(a)



(b)

Fig. 1. Cigre benchmark model for the low voltage μ -grid [1]
(a) Block diagram for the grid connected converter model (Converter A~E) (b) Single line diagram of LV micro-grid network model

II. SYSTEM DESCRIPTION

A Cigre benchmark model [1] is used as the principle reference network in order to increase the validity of the model. The block diagram of the LV network is shown in Fig. 1, where five power electronics converters are considered as the renewable energy sources and PI-section models are used the LV cable models between the converters and the feeder.

Table I. System parameter for benchmark model (see Fig. 1)

Conv.	A	B	C	D	E
P_{rate}	35 kVA	25kVA	3kW	4kW	10kW
L_f (mH)	0.87	1.2	5.1	3.8	0.8
R_{Lf} (m Ω)	11.4	15.7	66.8	49.7	10
C_f (uF)	22	15	2	3	15
R_{Cf} (m Ω)	7.5	11	21.5	14.5	11
L_g (mH)	0.22	0.3	1.7	1.3	0.2
R_{Lg} (m Ω)	2.9	3.9	22.3	17	2.5
V_{dc} (V)	750	750	750	750	750
C_{dc} (uF)	1000	1000	500	500	800
R_{dc} (Ω)	10	10	10	10	10
f_{sw} (kHz)	10	10	16	16	10

Additionally, the impedances of circuit breaker and contactor are not taken into account in the model. Even though the converters (A~E) in Fig 1-(a) are defined as specific renewable energy sources, the various combinations are also possible according to the conditions. The detailed information about the filter parameters and switching frequencies are shown in Table I, where the LCL circuit is considered as the filter for the connection of the power converter to the grid. The more detailed parameters for the low pass filter ($H_1(s), H_2(s)$) in Fig. 1-(a), the PI controller ($PI(s)$) and the Proportional Resonant Controller ($PR(s)$) are described in Section III.

III. HSS MODELING AND ANALYSIS OF MULTI-PARALLEL CONNECTED CONVERTER

A. Review of HSS modeling

The HSS modeling method is originally introduced to include time varying points of a linearized model. The Linear Time Varying (LTV) model is practically a non-linear model because of the varying characteristic of system parameters. Hence, it is difficult to be solved at a specific operating point as like the Linear Time Invariant (LTI) model. However, if all signals are assumed to be varying periodically, it is possible to linearize by means of Fourier series [16]. Based on these assumption and definitions, the HSS model can have a format as given in (1), where X_n is the harmonic state matrix, Y_n is the output harmonic matrix, U_m is the input harmonic matrix and A_{n-m} is the harmonic state transition matrix driven from the LTP theory [17]. $B_{n-m}, C_{n-m}, D_{n-m}$ are also a harmonic state matrix analogously, which is dependent on the number of input and output. The matrix size is dependent on the number of harmonics considered in the HSS modeling procedure. In this paper, “+40th ~ -40th” harmonic are considered in order to see the harmonic coupling of the 40th harmonic, where this is based on the assumption that the harmonics above 2 kHz are out of interest because of control bandwidth and also the inherent damping of micro-low voltage grid.

$$\begin{aligned} (s + jm\omega_0)X_n &= \sum_{m=-\infty}^{\infty} A_{n-m}X_m + \sum_{m=-\infty}^{\infty} B_{n-m}U_m \\ Y_n &= \sum_{m=-\infty}^{\infty} C_{n-m}X_m + \sum_{m=-\infty}^{\infty} D_{n-m}U_m \end{aligned} \quad (1)$$

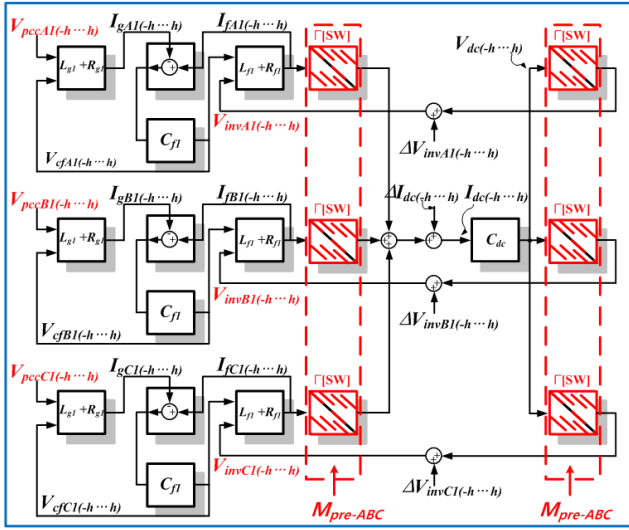


Fig 2. A single 3-phase PWM converter (topology) using HSS modeling.

B. 3-phase grid connected converter

Based on (1), a 3-phase grid connected PWM converter is modeled, where the detailed procedure for controller is modeled according to the procedure described in [18]. The modeling results are shown in (2) - (4), where, “ I ” means the identity matrix, “ Z ” is the zero matrix and “ N ” is the dynamic matrix, which is derived from (1). The time domain switching function is reorganized into a Toeplitz (Γ) [19] matrix in order to perform a convolution by means of the method described in Fig. 2. The small letter in Fig. 1-(a) means the time domain signal. The capital letters in Fig. 2 and (2) stand for the harmonic coefficient component, which is derived from the Fourier series. The final block diagram of the 3-phase grid connected PWM converter is shown in Fig. 2.

$$\begin{bmatrix} I_{g-abc}(t) \\ I_{f-abc}(t) \\ V_{cap-abc}(t) \\ V_{dc}(t) \end{bmatrix} = \begin{bmatrix} -\frac{R_g}{L_g}I - N & 0 & \frac{1}{L_g}I & 0 \\ 0 & -\frac{R_f}{L_f}I - N & \frac{1}{L_f}I & -\frac{\Gamma[SW]^T}{L_f} \\ \frac{1}{C_f}I & \frac{1}{C_f}I & -N & 0 \\ 0 & \frac{\Gamma[SW]}{C_{dc}} & 0 & -N \end{bmatrix} \begin{bmatrix} I_{g-abc}(t) \\ I_{f-abc}(t) \\ V_{cap-abc}(t) \\ V_{dc}(t) \end{bmatrix} + \begin{bmatrix} \frac{1}{L_g}I \\ 0 \\ 0 \\ 0 \end{bmatrix} [V_{pcc-abc}(t)] \quad (2)$$

The harmonic coefficient vector from PCC ($V_{pccABC1(-h...h)}$) is transferred into the LCL-filter side using the harmonic transfer function. The calculated harmonic vector of the converter side filter current ($I_{fABC1(-h...h)}$) is transferred into the dc-side harmonic transfer function through

a linearized switching harmonic vector ($\Gamma[SW]$). The summation of each phase current ($I_{gABC1(-h...h)}$) is a dc current harmonic vector ($I_{dc1(-h...h)}$), where this is convoluted with the dc network harmonic vector (C_{dc}) in order to get a dc voltage harmonic vector ($V_{dc1(-h...h)}$). The results are then convoluted again with the switching harmonic vector ($\Gamma[SW]$) in order to obtain the harmonic vector of the inverter side voltage ($V_{invABC1(-h...h)}$). The derived harmonic vector of the converter side voltage is transferred to the LCL - filter side harmonic transfer function, repetitively, in order to get the response of each harmonic vector.

D. Low voltage cable

In order to consider the interaction from the cables, this is also modeled. Instead of using a simple inductance or resistance model, a PI-section model is used dependent on the length. The derived result is shown in Fig. 3, where the HSS modeling theory (1) is used to include the harmonics in the model. The G_{PI} , C_{PI} , L_{PI} , R_{PI} are conductance, capacitance, inductance and resistance of the PI-section cable model, respectively. However, the conductance is not taken into account of the parameters and the capacitance is determined by an assumed value. As a result, the cable model for 1-phase can be obtained as given by Fig. 3, (3). In addition, the acronyms and subscripts used in (3) have also same meaning as with (2). The obtained cable model is combined with the other converters as shown in Fig. 1. (C1 - C9).

$$\begin{bmatrix} V_{pcc}(t) \\ V_{FEED}(t) \\ I_L(t) \end{bmatrix} = \begin{bmatrix} \text{diag}\left(-\frac{G_{PI}}{C_{PI}}\right) - N & Z & \text{diag}\left(-\frac{2}{C_{PI}}\right) \\ Z & \text{diag}\left(-\frac{G_{PI}}{C_{PI}}\right) - N & \text{diag}\left(\frac{2}{C_{PI}}\right) \\ \text{diag}\left(\frac{1}{L_{PI}}\right) & \text{diag}\left(-\frac{1}{L_{PI}}\right) & \text{diag}\left(-\frac{R_{PI}}{L_{PI}}\right) - N \end{bmatrix} \begin{bmatrix} V_{in}(t) \\ V_{out}(t) \\ I_L(t) \end{bmatrix} + \begin{bmatrix} \text{diag}\left(\frac{2}{C_{PI}}\right) & Z \\ Z & \text{diag}\left(-\frac{2}{C_{PI}}\right) \\ Z & Z \end{bmatrix} \begin{bmatrix} I_{in-cable}(t) \\ I_{out-cable}(t) \end{bmatrix} \quad (3)$$

The developed HSS model for the cable can also be used for the other phases. The used cable data are as follows [20]:

- Current Rating : 200A
- Cable Type : 3-Conductor A1-PVC 185mm²
- Resistance : 0.152 mΩ/meter
- Inductance : 0.237 uH/meter
- Capacitance : 2 pF/meter (assumed)
- Cable length : 100 m (C1~C9) (assumed)

IV. SIMULATION AND EXPERIMENTAL RESULTS

To validate the modeling and analysis results of parallel converters, MATLAB and PLECS are used for the time and frequency domain simulations to be used for two different assessment methods. Laboratory tests are also performed in an experimental set-up, where three 3-phase frequency converters are used as the PWM converters. The control algorithms are implemented in a DS1007 dSPACE system without harmonic

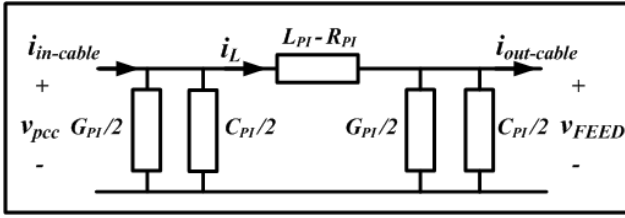


Fig 3. PI section model for 1-phase cable.

compensator in order to see the harmonic components. The model of grid is used to see the harmonic performance.

A. Simulation from the HTF (Harmonic Transfer Function)

Describing both the steady-state and dynamic harmonic coupling is possible by means of the modeling method from (1), where it can be converted into the harmonic transfer function ($H_k(s)$) format for each harmonic component (k) by using (4).

$$H_k(s) = \sum_l \hat{C}_{k-l} \left((s + j\omega_0)I - \hat{A} \right)^{-1} \hat{B}_l + D_k \quad (4)$$

where, \hat{B}_k , \hat{C}_k , and D_k , are the Fourier coefficients of the periodic functions $\hat{B}(t)$, $\hat{C}(t)$, and $D(t)$, respectively. At this point, $H(s)$ is a doubly infinite matrix, where this defines the coupling between different frequencies. When “s” is equal to “0”, it can show the steady state harmonic coupling. When s is non-zero, it can explain the dynamic interaction between the coupled harmonic transfer functions. Hence, this is enough to show the stability and impedance coupling in the system [17].

Based on (4), a mapping example for the steady state harmonic coupling between 5 parallel converters is shown in Fig 4, where each dot (•) means the harmonic impedance and the Jacobian values of each harmonic impedances. Due to the visibility of the coupling map, only the 5th harmonic is considered in this mapping. However, the number of harmonics can be increased according to the harmonics of interest. The mapping for the harmonics coupling show intuitively how the input grid voltage harmonics are coupled with the output harmonics through the harmonics impedance. The minus (-) and plus (+) harmonics in the harmonic vector are the complex conjugates, which also composed to the positive, negative and zero sequence. Hence, if the-3 phase system is in the balanced, the output harmonics are also balanced. As the harmonic impedance can be canceled out due to the conjugate characteristics, even if there are harmonics impedance in the map. However, in the case of the unbalanced parameters, the harmonic impedance of the positive, negative and zero sequence can not be canceled out. Therefore, the results of the output harmonics can have harmonics, which are driven by unbalanced parameters. The steady state results from Fig. 4 are shown in Fig. 6 where the harmonics are generated due to the relation in the harmonic coupling seen in Fig. 4.

To decide the dynamic characteristic of each harmonics, the harmonic transfer functions of 5 parallel converters are shown in Fig 5, where the results are obtained by using (4). The converters (1-5) have different harmonic transfer

functions according to the system parameter given by Table I. The characteristic of the harmonic transfer functions is also different due to the load variations as shown in Fig 5-(c), (d). In 50 Hz~100 Hz (red circle), the characteristic of the transfer function is changed, which affects the transient status of the dc circuit and the grid voltage. As a result, this characteristic shows a difference with the LTI model, where the transfer function derived from the LTI model does not care about both the input information and the dc side circuit. Furthermore, it can be found that the dynamics of each phase are also different in 50 Hz ~100 Hz (red-circle) as shown in Fig. 5-(a), (b), which shows that the impedance characteristic driven by the LTI model can not cover these differences.

Based on the steady-state harmonic impedance and the dynamic harmonic transfer function as given by Fig. 4 and Fig. 5, the dynamic performance of the grid current, dc voltage and dc current are evaluated. By using the harmonic vector of the grid voltage and dc reference as the input, the output current - harmonic vectors of 5 parallel converters can be obtained from the harmonic transfer function. The calculated harmonics vector can be transformed into the time domain data by means of a phasor rotation. The simulated results are shown in Fig. 8, where the 3-phase grid current of the 5 parallel converters and the dc-voltage / current of the 5 parallel converters are evaluated according to the parameters given in Table I. In Fig. 6, the steady-state waveforms from 0.4 sec to 0.5 sec are the same as the results, which are derived from the harmonic coupling map (harmonic domain) in Fig. 4. However, the dynamic transients at 0.5 sec are derived from the harmonic transfer function in Fig. 5. Therefore, the dc voltage, current and grid current show the different dynamics in Fig. 6 according to the different harmonic transfer function in Fig. 5, where the harmonic transfer function can be changed as shown in Fig. 5-(c) and Fig. 5-(d). As a result, the updated harmonic transfer function shows exactly the same time-domain results as shown in Fig. 6.

B. Experimental validation

An experimental set-up for the validation of the proposed model is shown in Fig. 7 where 3 parallel grid connected converters are used to compare the results. However, the cables are not considered in the experiment. The interface between the hardware and controller is that signals (yellow line) are sensed and sampled by dSPACE. Then, by using the control algorithm given in Fig. 1 and the sampled signals, which are implemented in the Control Desk of the dSPACE, the PWM signals (red-line) for 3 converters can be generated. The data exchange (green-line) between Control Desk and the dSPACE are done by a LAN cable.

Even though a direct method to measure the impedance is to use a perturbation and observe the response in order to verify the model, the impedance is not directly measured in this paper. Due to the difficulties in measuring the multiple impedances, the proposed model (2) - (4) is verified by using the measured signals only. The test sequence is as follows:

1. The 3-converter should operate at steady state in order to obtain the periodic signals.

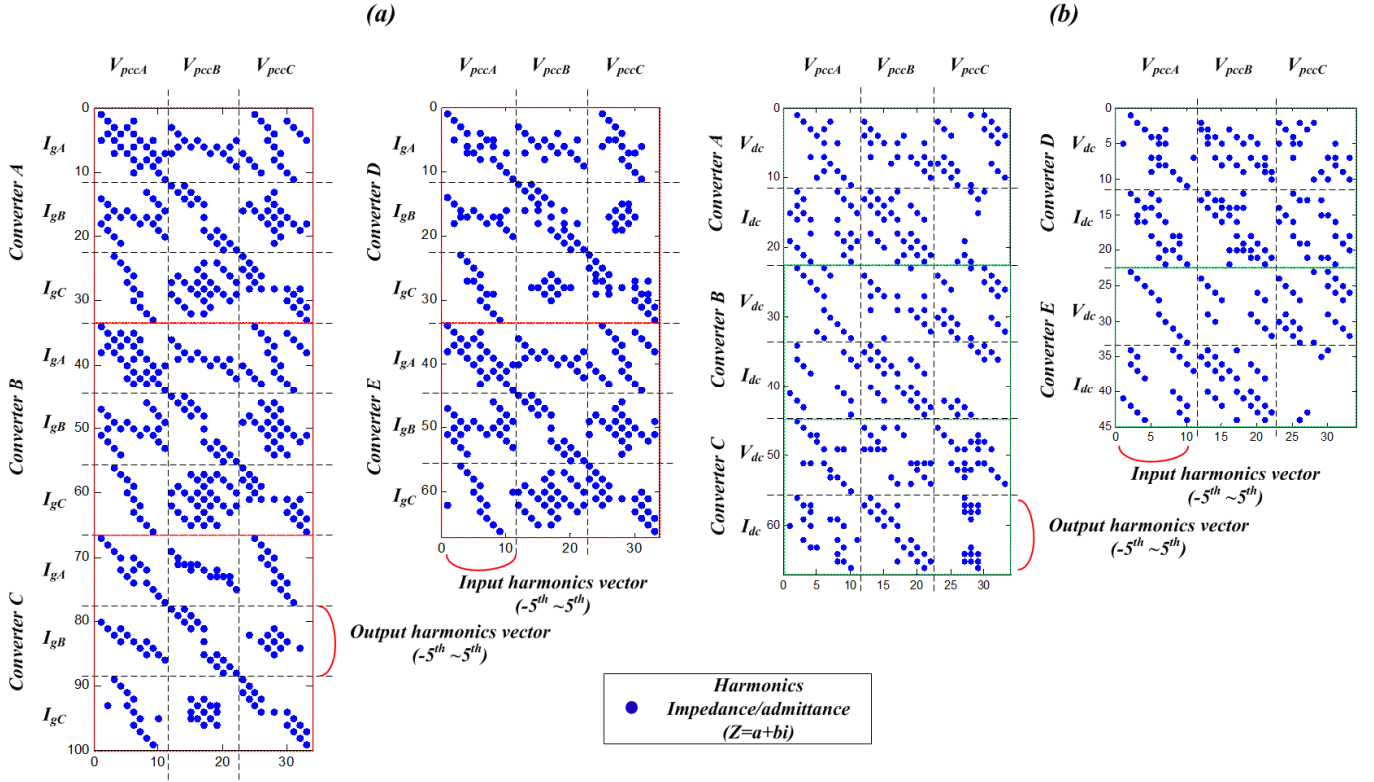


Fig 4. Jacobian sparse matrix (Harmonic domain) from (12) for 5 grid converters, where X and Y axis is the harmonic vector ($-5^{th} \sim 5^{th}$).

(a) Harmonic coupling of grid voltage ($V_{line-ABC}$) to grid current (I_{g-ABC}),

(b) Harmonics coupling of grid voltage ($V_{line-ABC}$) to dc voltage (V_{dc}) and dc current (I_{dc})

2. The grid current (i_g), the converter side current (i_f), the voltage of the filter capacitor (v_f), and the state of the controller etc., can be obtained by using the recording function in dSPACE.

3. The obtained steady state signals should be converted to the Fourier coefficient by using the Discrete Fourier Transform (DFT) in order to get the previous state and the nominal values of the converter model. It is noted that the synchronization is important in the measurement in order to acquire an accurate verification.

4. The calculated Fourier coefficients can be the previous state values and the nominal values of the developed HSS models. Hence, based on the measured Fourier coefficients, the time-varying output harmonic coefficient can be obtained from the HSS model.

5. The final Fourier coefficient can be transformed into the time-domain signals by rotating the signals with the specific frequency.

6. The calculated response from the HSS model and the measured results from the oscilloscope can be compared for validation.

According to the described procedure, the calculated and experimental results are compared, where the detailed parameters for a 1 kW power rating is shown in Fig. 8. The measured signals from the dSPACE recording function can be transformed into a DFT format. By inserting these harmonic

vectors into the developed harmonic transfer function as the nominal system value, the output harmonic vector of the current can be obtained. As a result, the final waveforms are compared with PLECS and the experimental results are as shown in Fig. 8. Even though small errors can be found at the even harmonics, the other characteristic harmonics coming from the modulation are well seen in the experimental results.

V. CONCLUSION

This paper analyzes the harmonic coupling in multiple parallel connected converter systems by using an HSS modeling approach. The modeling and simulation results show how important harmonics below the 20th order are generated in each converter. The modeling can also explain how the output current harmonics of each converter is coupled to each other with other paralleled connected converters. Furthermore, this model can explain that the dynamic performance dependent on the dc-operating point is not only one to explain the complex parallel system, where there is another possibility due to the dominant harmonic impedance at specific frequency. The results show that the responses of each harmonic have different characteristic which is not seen in the classical model. The multiple transfer functions, which consider the varying operating point, can be used for the analysis of the harmonic coupling in a large network. e.g. Cigre low voltage micro grid network model.

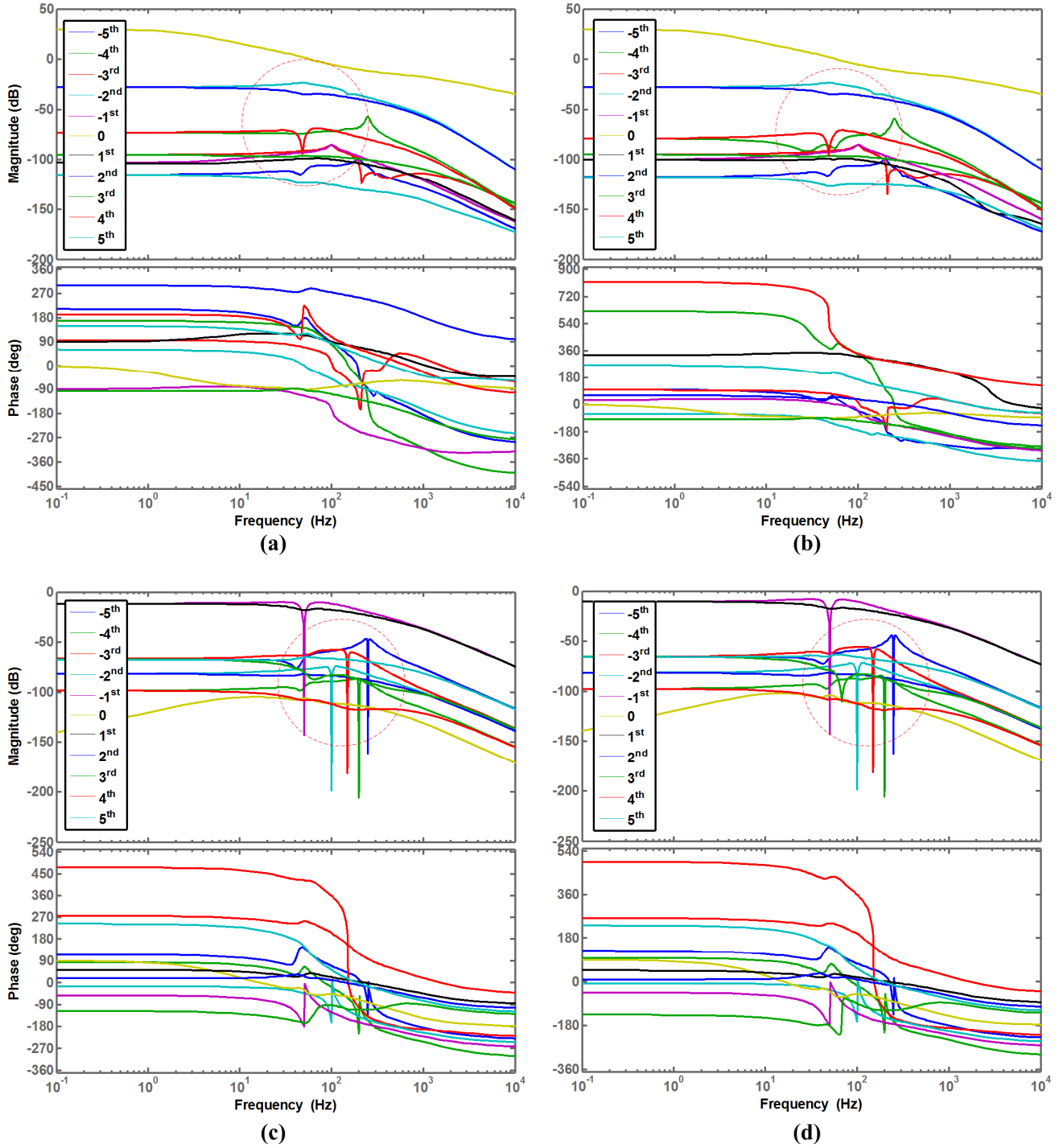


Fig 5. Closed loop Harmonic Transfer Function of 5 paralleled converters (parameters are given in Table I)

(a) Converter - A (I_{g-A}/V_{pcc-A}), (b) Converter - A (I_{g-B}/V_{pcc-B}),
(c) Converter - A (V_{dc-A}/V_{pcc-A}), $I_{dc-load} = 75A_{dc}$, (d) Converter - A (V_{dc-A}/V_{pcc-A}), $I_{dc-load} = 13A_{dc}$,

ACKNOWLEDGMENT

This work was supported by European Research Council under the European Union's Seventh Framework Program (FP/2007-2013)/ERC Grant Agreement n. [321149-Harmony].

REFERENCES

- [1] C. T. Force, "Benchmark Systems for Network Integration of Renewable Energy Resources," in *CIGRE Task force C6.04.02.*, ed: CIGRE, 2011.
- [2] X. Wang, F. Blaabjerg, and W. Weimin, "Modeling and Analysis of Harmonic Stability in an AC Power-Electronics-Based Power System," *IEEE Trans. on Power Electron.*, vol. 29, pp. 6421-6432, 2014.

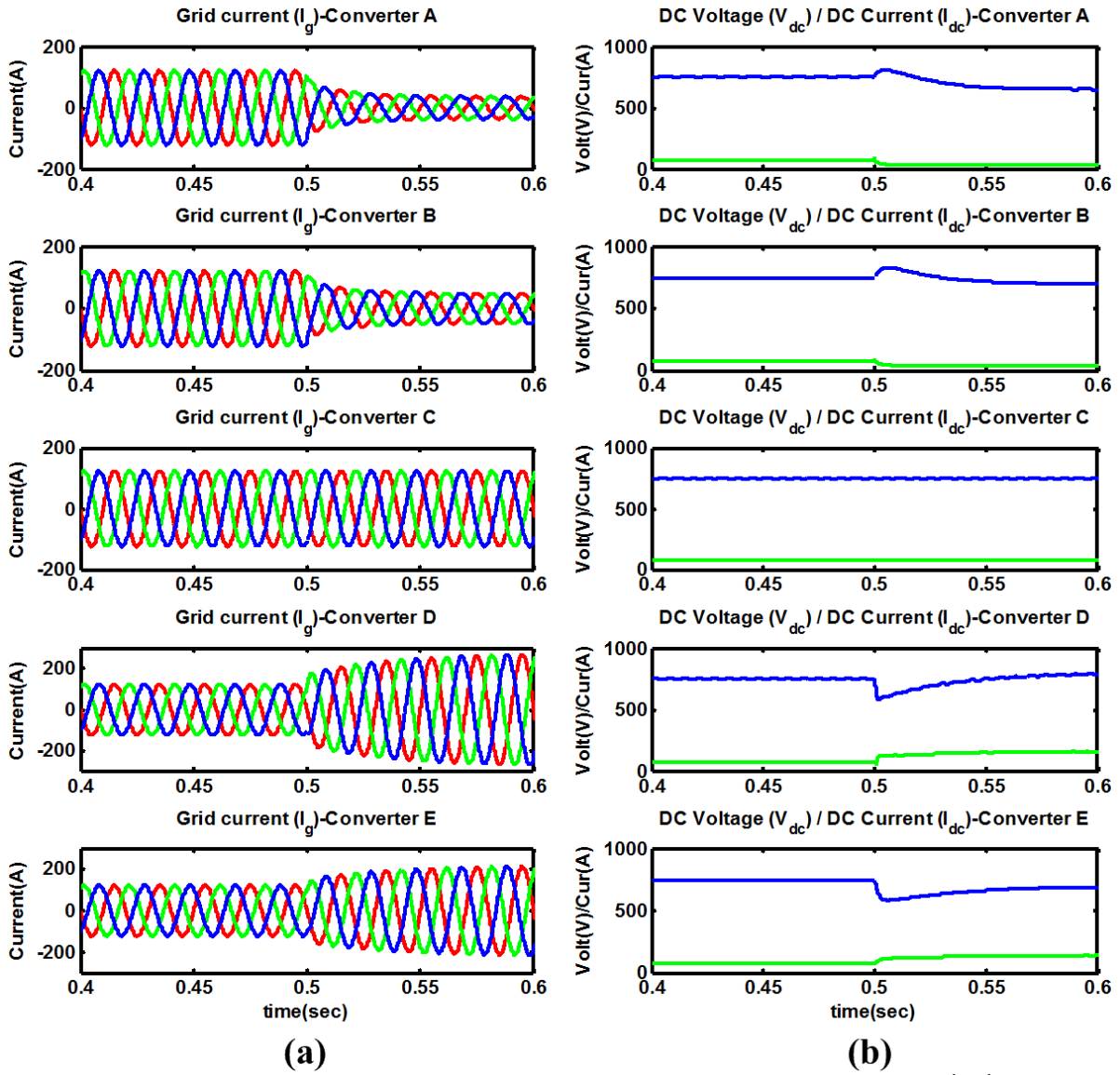


Fig 6. Time domain simulation results from the Harmonic Transfer Function ($h = -5^{th} \sim 5^{th}$)

(a) Grid current (I_g) of Converter A,B,C,D,E, (b) DC voltage (V_{dc}) and DC current (I_{dc}) of Converter A,B,C,D,E

(From 0.4~0.5 sec, the parameters are same with Table I. The dc load current and dc voltage reference are changed at 0.5 sec :

Converter A ($V_{dc}^* = 650 / R_{dc} = 50$ ohm), Converter B ($V_{dc}^* = 700 / R_{dc} = 20$ ohm), Converter C ($V_{dc}^* = 750 / R_{dc} = 10$ ohm), Converter D ($V_{dc}^* = 800 / R_{dc} = 5$ ohm), Converter E ($V_{dc}^* = 700 / R_{dc} = 5$ ohm)), where R_{dc} is the dc load.

- [3] N. Krutikova, C. A. Hernandez-Aramburo, and T. C. Green, "State-space model of grid-connected inverters under current control mode," *Electric Power Applications, IET*, vol. 1, pp. 329-338, 2007.
- [4] N. Pogaku, M. Prodanovic, and T. C. Green, "Modeling, Analysis and Testing of Autonomous Operation of an Inverter-Based Microgrid," *IEEE Trans. Power Electron.*, vol. 22, pp. 613-625, 2007.
- [5] C. Meyer, M. Hoing, A. Peterson, and R. W. De Doncker, "Control and Design of DC Grids for Offshore Wind Farms," *IEEE Trans. Ind. Appl.*, vol. 43, pp. 1475-1482, 2007.
- [6] L. Yazhou, A. Mullane, G. Lightbody, and R. Yacamini, "Modeling of the wind turbine with a doubly fed induction generator for grid integration studies," *IEEE Trans. Energy Conv.*, vol. 21, pp. 257-264, 2006.
- [7] J. L. Agorreta, M. Borrega, Lo, x, J. pez, and L. Marroyo, "Modeling and Control of N-Paralleled Grid-Connected Inverters With LCL Filter Coupled Due to Grid Impedance in PV Plants," *IEEE Trans. Power Electron.*, vol. 26, pp. 770-785, 2011.
- [8] S. R. Sanders, J. M. Noworolski, X. Z. Liu, and G. C. Verghese, "Generalized averaging method for power conversion circuits," *IEEE Trans. Power Electron.*, vol. 6, pp. 251-259, 1991.
- [9] M. Cespedes and S. Jian, "Impedance Modeling and Analysis of Grid-Connected Voltage-Source Converters," *IEEE Trans. Power Electron.*, vol. 29, pp. 1254-1261, 2014.
- [10] F. Castro Sayas and R. N. Allan, "Generation availability assessment of wind farms," *Generation, Transmission and Distribution, IEE Proceedings*, vol. 143, pp. 507-518, 1996.

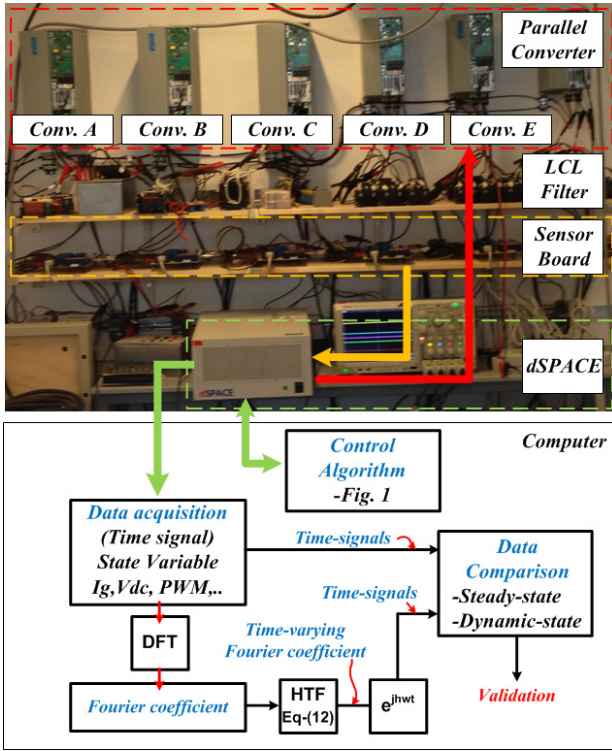


Fig 7. Experimental set up and the sequence for validation of the harmonic transfer function

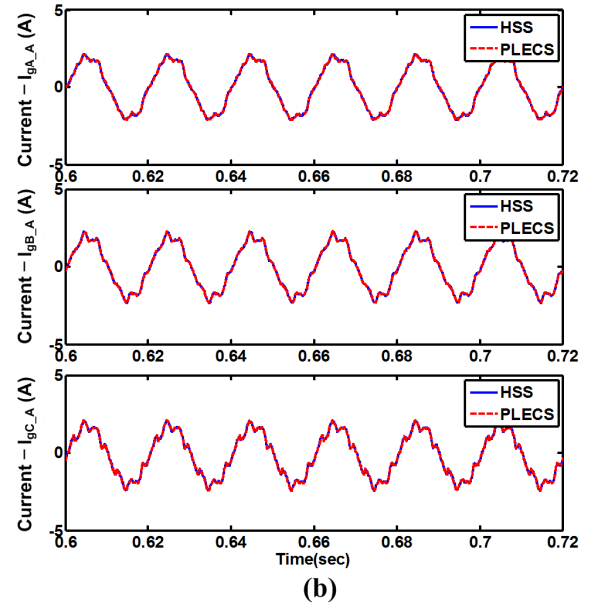
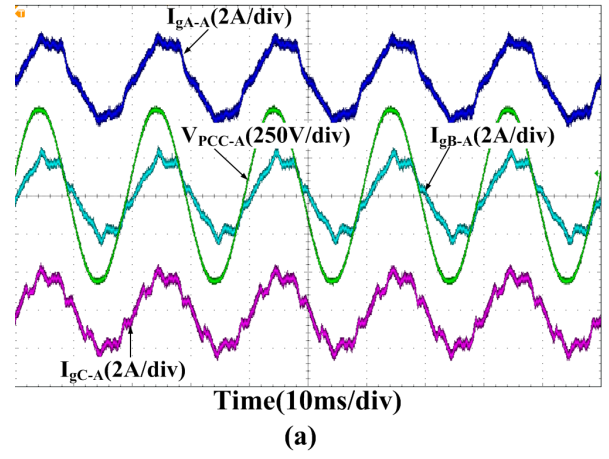


Fig 8. Simulation and experimental results at 1kW Power rating using HSS modeling and PLECS

Converter-1 : $L_f = 3 \text{ mH}$, $L_g = 1 \text{ mH}$, $C_f = 4.7 \mu\text{F}$, $C_{dc} = 450 \mu\text{F}$, $V_{pcc(\text{line-line})} = 380 \text{ V}$, switching frequency = 10 kHz
 Converter-2 : $L_f = 1.5 \text{ mH}$, $L_g = 1.5 \text{ mH}$, $C_f = 4.7 \mu\text{F}$, $C_{dc} = 450 \mu\text{F}$, $V_{pcc(\text{line-line})} = 380 \text{ V}$, switching frequency = 10 kHz
 Converter-3 : $L_f = 0.7 \text{ mH}$, $L_g = 0.3 \text{ mH}$, $C_f = 4.7 \mu\text{F}$, $C_{dc} = 450 \mu\text{F}$, $V_{pcc(\text{line-line})} = 380 \text{ V}$, switching frequency = 10 kHz

- Grid side inductor current simulation (harmonic = $-40^{\text{th}} \sim 40^{\text{th}}$) waveform (a) Experimental results (blue = grid side current (I_{gA-A}), cyan = grid side current (I_{gB-A}), purple = grid side current (I_{gC-A}), green = grid voltage (V_{pcc-A}))

(b) Simulation results (grid side current (I_{gA-A}), grid side current (I_{gB-A}), grid side current (I_{gC-A}))

- [11] J. Skea, D. Anderson, T. Green, R. Gross, P. Heptonstall, and M. Leach, "Intermittent renewable generation and maintaining power system reliability," *Generation, Transmission & Distribution, IET*, vol. 2, pp. 82-89, 2008.
- [12] M. S. P. Hwang and A. R. Wood, "A new modelling framework for power supply networks with converter based loads and generators - the Harmonic State-Space," in *Proc. IEEE POWERCON*, 2012, pp. 1-6.
- [13] J. Arrillaga and N. R. Watson, "The Harmonic Domain revisited," in *Proc. IEEE ICHQP*, 2008, pp. 1-9.
- [14] B. Vyakaranam, M. Madrigal, F. E. Villaseca, and R. Rarick, "Dynamic harmonic evolution in FACTS via the extended harmonic domain method," in *Proc. IEEE PECE*, 2010, pp. 29-38.
- [15] E. Mollerstedt and B. Bernhardsson, "Out of control because of harmonics-an analysis of the harmonic response of an inverter locomotive," *IEEE Trans. on Control Sys.*, vol. 20, pp. 70-81, 2000.
- [16] N. M. Wereley and S. R. Hall, "Frequency response of linear time periodic systems," in *Proc. IEEE CDC*, 1990, pp. 3650-3655 vol.6.
- [17] N. M. Wereley and S. R. Hall, "Linear Time Periodic Systems: Transfer Function, Poles, Transmission Zeroes and Directional Properties," in *Proc. IEEE ACC*, 1991, pp. 1179-1184.
- [18] J. Kwon, X. Wang, C. L. Bak, and F. Blaabjerg, "Harmonic Interaction Analysis in Grid Connected Converter using Harmonic State Space (HSS) Modeling," in *Proc. IEEE APEC 2015*.

- [19] J. R. C. Orillaza and A. R. Wood, "Harmonic State-Space Model of a Controlled TCR," *IEEE Trans. Power Deliv.*, vol. 28, pp. 197-205, 2013.
- [20] S. Anand and B. G. Fernandes, "Reduced-Order Model and Stability Analysis of Low-Voltage DC Microgrid," *Industrial Electronics, IEEE Transactions on*, vol. 60, pp. 5040-5049, 2013.